JGR Earth Surface

RESEARCH ARTICLE
10.1029/2022JF006906

Iron Loss During Continental Weathering in the Early Carboniferous Period Recorded by Karst Bauxites

Kunyue Ling[1], Hanjie Wen[2,3], Haifeng Fan[1], Xiangkun Zhu[4], Zhihong Li[4], Zhengwei Zhang[1], and Stephen E. Grasby[5]

[1]State Key Laboratory of Ore Deposit Geochemistry, Institute of Geochemistry, Chinese Academy of Sciences, Guiyang, China, [2]School of Earth Science and Resources, Chang'an University, Xi'an, China, [3]College of Earth and Planetary Sciences, University of Chinese Academy of Sciences, Beijing, China, [4]MNR Key Laboratory of Deep-Earth Dynamics, MNR Key Laboratory of Isotope Geology, Institute of Geology, Chinese Academy of Geological Sciences, Beijing, China, [5]Geological Survey of Canada, Calgary Natural Resources Canada, Calgary, AB, Canada

Key Points:

- Fe-poor bauxite is enriched in heavy Fe isotopes due to the release of isotopically light dissolved Fe(II) during pedogenesis
- Most dissolved Fe(II) was rapidly oxidized to Fe(III) and transported toward the continental margin forming iron ores
- Karst bauxite in southwestern China may have recorded Fe loss during continental weathering

Supporting Information:

Supporting Information may be found in the online version of this article.

Correspondence to:

K. Ling and H. Wen,
lingkunyue@mail.gyig.ac.cn;
wenhanjie@vip.gyig.ac.cn

Citation:

Ling, K., Wen, H., Fan, H., Zhu, X., Li, Z., Zhang, Z., & Grasby, S. E. (2023). Iron loss during continental weathering in the early Carboniferous period recorded by karst bauxites. *Journal of Geophysical Research: Earth Surface*, *128*, e2022JF006906. https://doi.org/10.1029/2022JF006906

Received 31 AUG 2022
Accepted 14 MAR 2023

Abstract Significant iron (Fe) loss can occur during continental weathering and efflux to the ocean via runoff, historically affecting global Fe cycling and marine ecosystems. Here, we report extremely low Fe content in early Carboniferous (ca. 340 Ma) bauxites in southwestern China. These bauxites were formed by redeposition of terrestrial soils along the paleo-continental margin of the western South China Plate in warm climates. The bauxites contain high δ^{56}Fe (−0.17‰ to +1.15‰) values with a negative correlation between Fe_2O_3 and δ^{56}Fe, indicating that a substantial amount of Fe(III) was reduced to isotopically light dissolved Fe(II) and effuxed to the ocean via reductive dissolution under anoxic conditions. The low C_{org} content and low Fe_{HR}/Fe_T, Mo/Al, U/Al, and V/Al ratios of bauxite suggest that this reduction process occurred during the pedogenic (continental weathering) rather than the depositional/diagenetic stage of karst bauxite formation. Most of the dissolved Fe(II) were rapidly re-oxidized to Fe(III) and transported toward the paleo-continental margin forming iron ores with δ^{56}Fe values around zero (−0.13‰ to +0.16‰). The negative correlation between Al_2O_3 and Fe_2O_3 contents in global karst bauxites suggests common Fe loss processes during continental weathering in geological periods favoring karst bauxite formation, such as during the Carboniferous, Permian, and Cretaceous periods and the Cenozoic era. Karst bauxite may thus provide a record of Fe loss during continental weathering and act as an indicator of enhanced Fe flux to oceans.

Plain Language Summary Bauxite deposits are weathered residues enriched in aluminum (Al). They are of economic importance and record critical information concerning extensive weathering in geological history. Karst bauxite has extremely low iron (Fe) contents, and the mechanism of Fe loss is poorly understood. We observed high δ^{56}Fe values in the early Carboniferous period (ca. 340 Ma) karst bauxite in southwestern China, suggesting the bauxite formation under water-saturated anoxic conditions with extensive loss of isotopically light Fe(II). Our results indicate strong decoupling of Fe and Al during the formation of karst bauxite, which may thus act as an indicator of Fe loss during continental weathering.

1. Introduction

As a bioelement, iron (Fe) is involved in numerous physiological processes such as photosynthesis, respiratory functioning, and nitrogen fixation of plankton. As such, Fe plays an important role in marine ecosystems (Boyd & Ellwood, 2010). River input, continental marginal sediment Fe-release, submarine hydrothermal emission, and atmospheric dust deposition are the four principal sources of Fe to the ocean (Beard et al., 2003; Chen et al., 2020; Dale et al., 2015; Jickells et al., 2005; Raiswell and Canfield, 2012; Saito et al., 2013; Scholz, Schmidt, et al., 2019).

Continental weathering is a ubiquitous process occurring in the present and the past, forming soils, sediments, and sedimentary rocks. It shapes the continental crust and modifies its chemical composition by producing detrital materials and releasing ions into the hydrosphere over geological timescales (X. M. Liu et al., 2013; Sauzéat et al., 2015). The rate and type of continental weathering are an important part of the geochemical budget of all elements, including Fe (Pistiner & Henderson, 2003). During continental weathering, a large amount of Fe is released from the dissolution of primary minerals and transported to the ocean via rivers, which may play a key role in controlling the global Fe cycle and marine ecosystems (Sigman & Boyle, 2000; Wiederhold et al., 2007b).

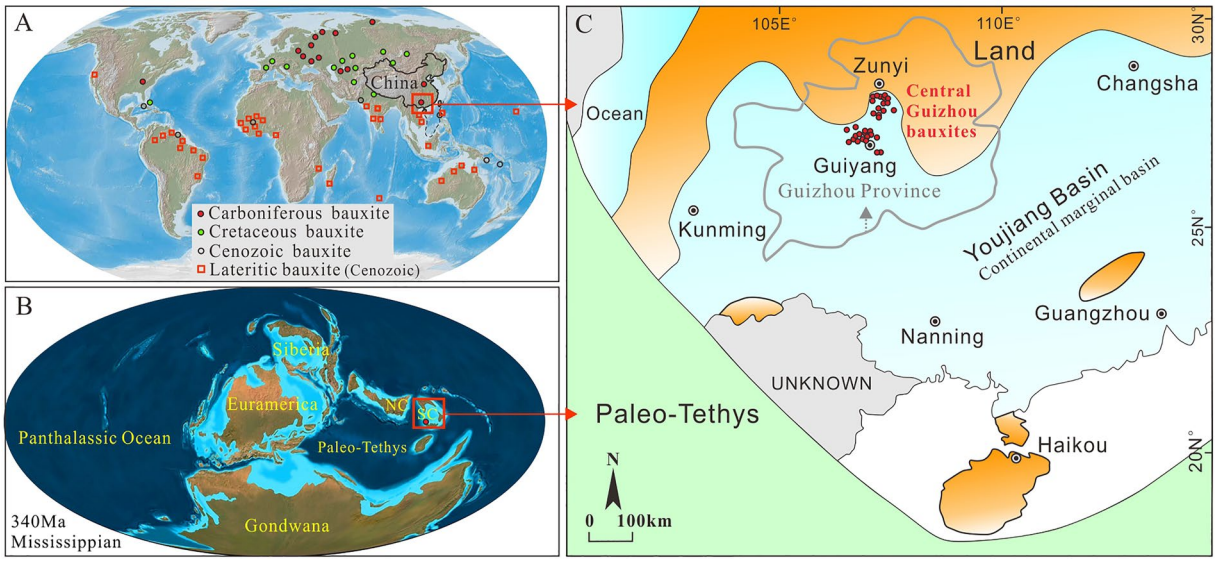

Figure 1. (a) World bauxite deposits, from Bogatyrev et al. (2009). (b) Mississippian paleogeography, courtesy of R. Blakey (http://jan.ucc.nau.edu/~rcb7/); bauxite deposits from Bogatyrev et al. (2009). (c) Paleogeographic map of the Youjiang Basin during the Early Carboniferous (Y. S. Ma et al., 2009).

Pioneering studies have documented that notable net Fe loss can occur during continental weathering and soil formation in (sub)tropical climate regions due to intensification of weathering with elevated temperature and rainfall (Akerman et al., 2014; S. Liu et al., 2014; Thompson et al., 2007; Wiederhold et al., 2006; Yesavage et al., 2012). These Fe were then delivered to the ocean through river systems and thus have a major impact on the global Fe cycle (Boyd & Ellwood, 2010; Tagliabue et al., 2014). The formation of Fe-poor soil associated with Fe loss is of great interest and has been used to study Fe migration and transformation at the Earth's surface (e.g., Thompson et al., 2007; Yamaguchi et al., 2007). However, it has also been argued that during extreme weathering under oxidative conditions, Fe is transformed into immobile ferric Fe and can be re-precipitated as Fe (hydr)-oxides (e.g., S. Liu et al., 2014; J. L. Ma et al., 2007; Poitrasson et al., 2008). It is an internal redistribution (closed-system) of Fe within the soil sections, resulting in limited Fe loss (M. Li et al., 2017; Qi et al., 2022). Therefore, the link between the Fe budget and continental weathering under (sub)tropical climates is not well established and requires further study.

Previous studies show that Fe loss is associated with the formation of bauxite deposits (e.g., Ling et al., 2017; Mameli et al., 2007). Bauxite is a (paleo-) chemical residue of intense subaerial weathering with Al_2O_3 contents of >35% and Al_2O_3/SiO_2 mass ratios of >2.6 (Bogatyrev et al., 2009). The link between bauxite deposits and tropical weathering regimes was established by Retallack (2010). Based on the lithology of the depositional basement, bauxite deposits are generally divided into three types (Bárdossy, 1982): (a) karst bauxite developed on the karstified surfaces of carbonate rocks; (b) lateritic bauxite developed on aluminosilicate rocks; and (c) Tikhvin bauxite representing transported and redeposited material overlying the eroded surface of aluminosilicate rocks. Karst bauxites are widely developed in Phanerozoic strata around the world, especially in the Carboniferous, Permian, Cretaceous periods, and Cenozoic era. The total karst bauxite resources exceed 10 billion tonnes (Figure 1, Bárdossy, 1982; Bogatyrev et al., 2009; Retallack, 2010). Bauxite deposits in China are dominated by the karst type and mainly of Carboniferous and Permian age found in the Guizhou, Guangxi, Shanxi, Henan Provinces, etc. (Deng et al., 2010; Q. Wang et al., 2020; S. Yang et al., 2022; Yu et al., 2019). Karst bauxites from China (especially central Guizhou bauxite) generally have much lower Fe_2O_3 contents (<2 wt. %, Ling et al., 2017) than other sediments/sedimentary rocks such as shale (North American Shale Composite (NASC) average 5.65 wt. %, Gromet et al., 1984). Central Guizhou karst bauxites were formed by the deposition of Al-rich soils in the early Carboniferous period on carbonate unconformities (basins) along the paleo-continental margin of the western South China Plate (Figures 1a–1c, Yu et al., 2019). They may have recorded ancient release of Fe during its formation and thus serve as an interesting target for studying earth-surface Fe cycling during extreme continental weathering in the geological past.

Fe has two valence states (Fe(II) and Fe(III)) and can produce large isotopic fractionation during redox reactions (Bergquist & Boyle, 2006). Fe(II) is generally more mobile and isotopically lighter than Fe(III) (John et al., 2012;

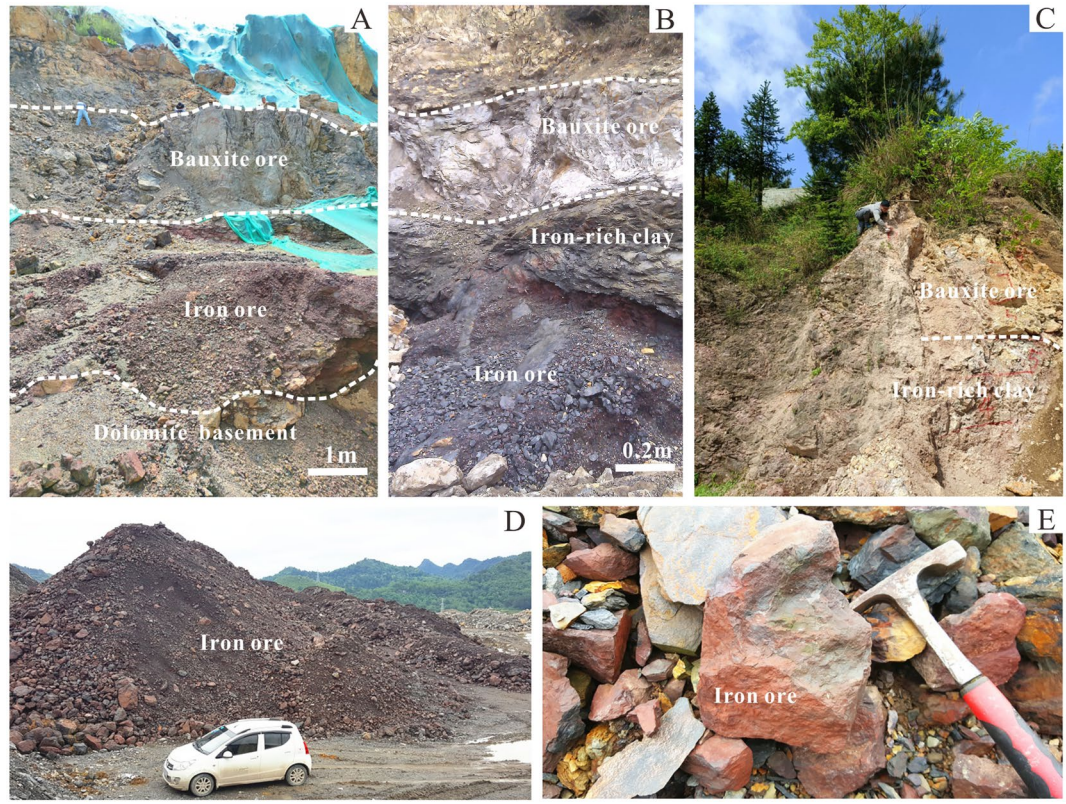

Figure 2. Field photos illustrating the contact relationship between iron bed (iron ore and iron-rich clay) and overlying bauxite bed (bauxite ore) in the central Guizhou area, SW China.

Teng et al., 2008). In surficial environments, this difference in mobility results in the release of light Fe isotopes into solution and the preferential sequestration of heavy Fe isotopes in the solid residue (e.g., Ilina et al., 2013; Johnson et al., 2008). Therefore, iron isotopes can provide deep insights into the mechanism of Fe mobilization (Rouxel et al., 2005).

As Fe-poor bauxite is a chemical residue of extreme weathering, studying the mechanism of Fe loss during karst bauxite formation could improve our understanding of the Earth-surface Fe cycling in tropical climate regions. To achieve this, we studied the isotopic composition of Fe in the early Carboniferous bauxites (ca. 340 Ma) from central Guizhou, southwestern China.

2. Geological Setting

The lower Carboniferous bauxite belt in central Guizhou, southwestern China, located in the western part of the South China Plate, contains more than 40 bauxite deposits with total resources exceeding 500 million tons (Figure 1a; Yu et al., 2019). During the Early Paleozoic, South China and North China plates separated from Gondwana and drifted northward (Metcalfe, 2006). During the early Carboniferous period, the South China Plate drifted close to the equator (Figure 1b) and experienced climatic warming, which was conducive to the formation of tropical soil via crustal weathering (Yu et al., 2019). During this period, Al-rich soils were transported mainly as suspended particulate matter (SPM) by rivers to the continental margin (Youjiang Basin; east Paleo-Tethys) and deposited in the Qingzhen-Xiuwen (Guiyang) and Zunyi coastal basins, forming the lower Carboniferous Jiujialu Formation bauxites in the central Guizhou area (Figure 1c, Yu et al., 2019).

The Jiujialu Formation, which shows parallel unconformities with the overlying lower Carboniferous limestone/clay rock and the underlying Cambrian or Ordovician dolomite strata, usually comprises a 1–20 m thick bauxite bed (bauxite ore/clay rock) and an underlying 0–6 m thick iron bed (iron ore/iron-rich clay) (Figure 2). This typical "iron-bauxite" structure is widespread worldwide, such as the Ghiona bauxite deposit in Greece (Kalaitzidis

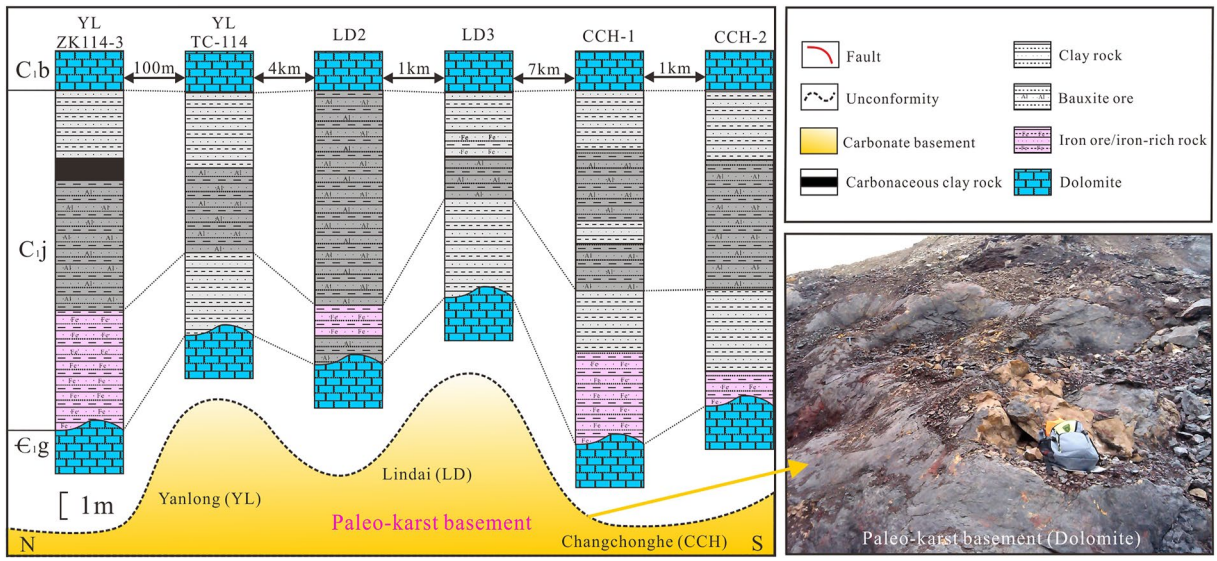

Figure 3. Stratigraphic columns of bauxite-bearing rock series in Lindai area, central Guizhou, SW China, illustrate the contact relationships between the depositional basement (paleo-karst), iron bed, and bauxite bed. Iron ore occurs only in karst depressions.

et al., 2010), the Nurra bauxite deposit in Italy (Mameli et al., 2007), the Kanisheeteh, Kanirash, Shahindezh, Qopi, Darzi-Vali; Soleiman-Kandi, Kani-Zarrineh bauxite deposits in Iran (Abedini, Habibi Mehr, et al., 2019; Abedini et al., 2019a, 2019b; Abedini et al., 2022a, 2022b; Calagari & Abedini, 2007; Khosravi et al., 2017, 2021), and most bauxite deposits in China (e.g., Ling et al., 2017; X. Liu et al., 2017; Yu et al., 2019; Z. Zhang et al., 2013). In central Guizhou, the thickness of the Jiujialu Formation is controlled by the paleo-karst unconformities, that is, the thickness above the karst depression is greater than that above the highland (Figure 3). The underlying strata (depositional basement of the Jiujialu Formation) include, from SW to NE, the Cambrian Series 2 Qingxudong Formation dolomite, Miaolingian Gaotai and Shilengshui formations dolomite, Miaolingian-Furongian Loushanguan Group dolomite, and Lower Ordovician Tongzi to Meitan formations dolomite and argillaceous rocks (Figure 4). The bauxites and clay rocks are usually off-white or ash-black in color and have clastic or compact textures (Figures 5a–5c), whereas the iron ores and iron-rich clays are brownish red or black and have compact textures (Figures 5d and 5e).

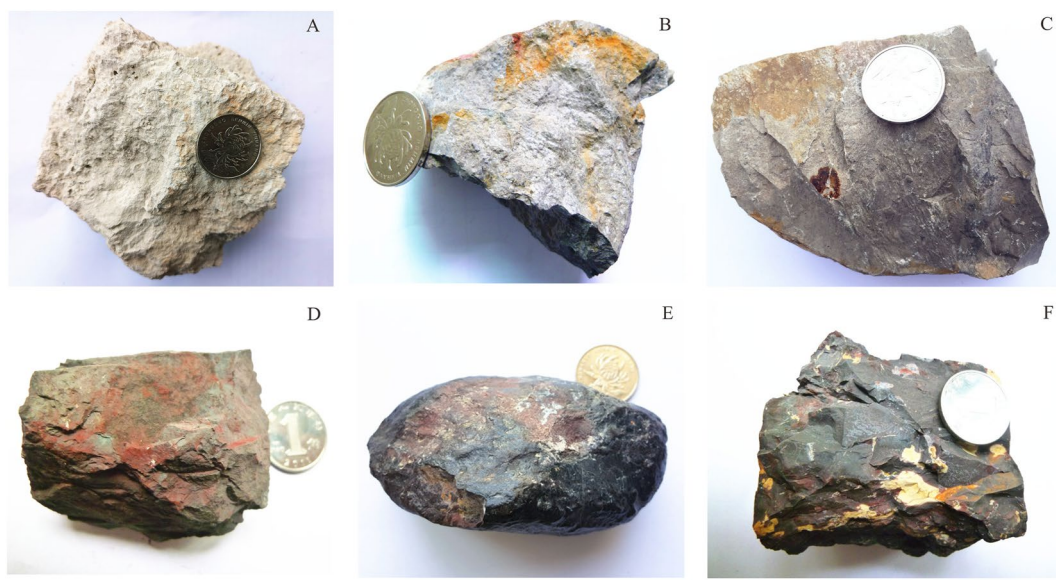

Figure 4. Photos of the bauxites from central Guizhou Province, Southwest China. (a–c) are bauxites and (d–e) are iron ores (hematite). (d) Is hematite-rich clay.

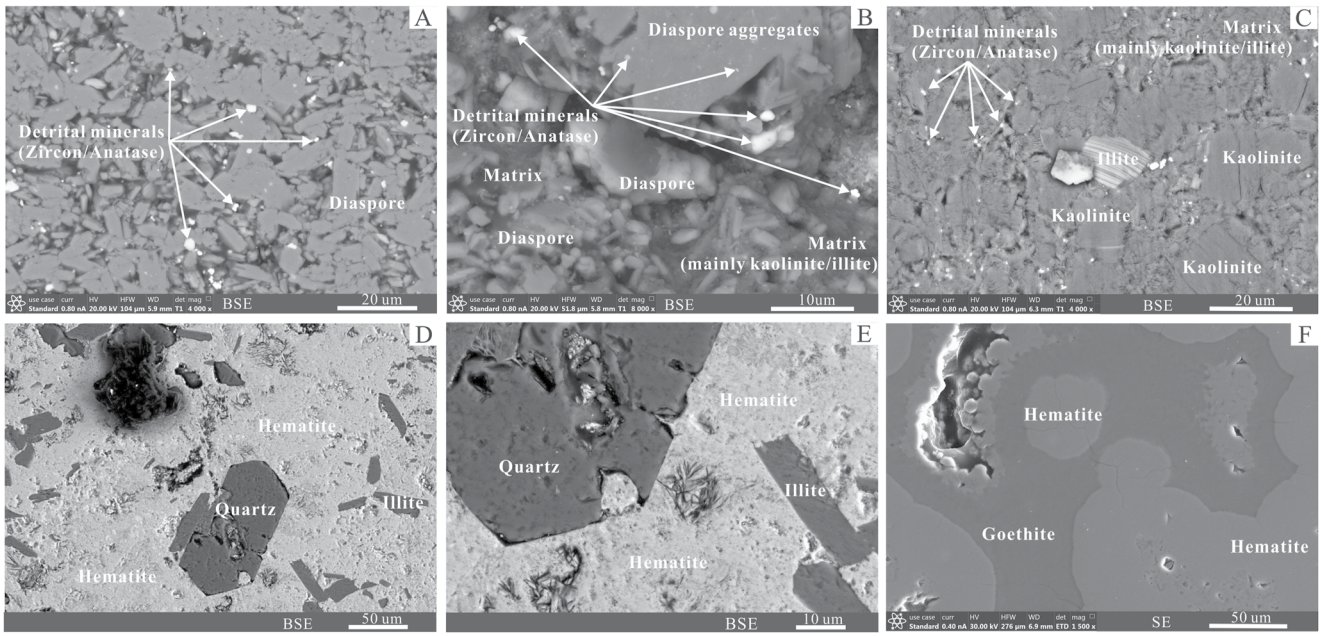

Figure 5. (a–b) Images of the bauxites, (c) clay rock, and (d–f) iron ores from central Guizhou Province, Southwest China. BSE: backscattered electron image. SE: secondary electronic images.

3. Sampling and Analytical Methods

A total of 68 samples from the lower Carboniferous Jiujialu Formation were collected in central Guizhou, southwestern China. Fresh rock samples from the Jiujialu Formation, including bauxites, bauxitic clays, clay rocks, iron ores, and iron-rich clays (Figure 4), were collected from outcrops and open pits at three bauxite deposits in the Guiyang area (Xiaoshanba, Lindai, and Yunwushan), and three bauxite deposits in the Zunyi area (Xinzhan, Houchao, and Xianrenyan) (Figure S1 in Supporting Information S1).

Polished thin sections were prepared for scanning electron microscope-energy dispersive spectrometer (SEM-EDS) analyses using a Thermo Scientific Scios DualBeam SEM-EDS at the Institute of Geochemistry, Chinese Academy of Sciences (IGCAS). Powdered samples were prepared for analyses of Al_2O_3, SiO_2, and Fe_2O_3 content ($n = 47$) at the IGCAS. The samples were washed, air-dried, powdered to 200 mesh, and homogenized prior to chemical analysis. Major element contents of whole-rock samples were determined by X-ray fluorescence (PANalytical, AXIOS-PW4400) at the IGCAS. The analytical precision is better than 5%. The trace element Mo, U, and V abundances were analyzed through whole-rock solution-ICP-MS techniques (PlasmaQuant MS Elite) at the IGCAS. The ICP-MS measurements were quality controlled using international standard samples OU-6, AMH-1, and GBPG-1, and the relative standard deviation was better than 10%. The organic carbon (C_{org}) analyses ($n = 29$) were conducted with an Elementar Vario Microcube analyzer at IGCAS, with analytical errors of less than ±2.5%. Prior to the analyses, the sample powders were leached with 2.5 N HCl to remove inorganic C. The Fe species extraction ($n = 29$) were performed at the China University of Geoscience. The Fe-pyrite fraction (Fe_{Py}) was calculated from Ag_2S produced by the chromous chloride distillation (Canfield et al., 1986). Fe-carbonate (Fe_{carb}; siderite and ankerite), Fe-oxide (Fe_{ox}; e.g., ferrihydrite, goethite and hematite), and Fe-magnetite (Fe_{mag}) species were extracted following the method established by Poulton and Canfield (2005). Fe contents were measured using atomic absorption spectrometry.

Iron isotopes ($n = 37$) were measured at the Laboratory of Isotope Geology, Institute of Geology, Chinese Academy of Geological Sciences. The detailed procedures for sample dissolution, chemical separation, and Fe isotope analysis were described by Sun et al. (2013). In brief, powdered samples were digested with HCl-HF-HNO_3, and Fe was chromatographically separated using an AG MP-1 M anion exchange resin loaded into low-density polyethylene columns. These processes yielded Fe recoveries of 99.7%–100% for the national basaltic standard reference material CAGSR-1 (GBW-07105). Iron isotopes were analyzed on a Neptune MC-ICP-MS using standard–sample bracketing. The external reproducibility of the isotopic measurements for the standard solutions

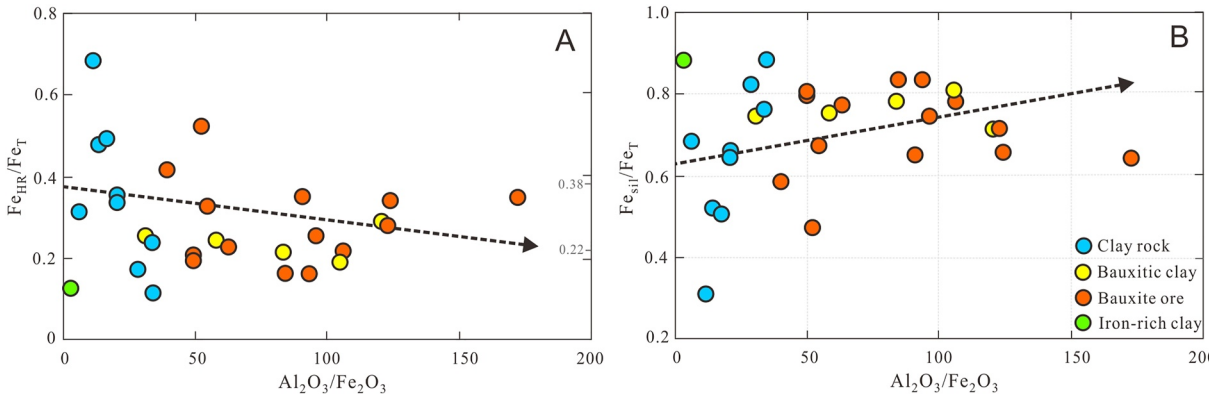

Figure 6. (a) Al_2O_3/Fe_2O_3 versus Fe_{HR}/Fe_T and (b) Fe_{sil}/Fe_T diagrams for central Guizhou bauxite samples. Fe_{HR}/Fe_T values of <0.22, 0.22–0.38, and >0.38 represent the oxic, possibly anoxic, and anoxic conditions, respectively (Poulton and Canfield, 2011). Since the formation of karst bauxite is a process of Fe loss and Al retention, the Al_2O_3/Fe_2O_3 value can be used to assess the mineralization degree of bauxite; that is, the higher the Al_2O_3/Fe_2O_3 value, the higher the mineralization degree.

was better than ±0.1% (2σ; n = 90 in one year, Zhu et al., 2008). The Fe isotope compositions are reported relative to the international standard IRMM-014 as follows: $\delta^{56}Fe_{IRM\text{-}014}$ (‰) = $[(Fe^{56}/Fe^{54})_{sample}/(Fe^{56}/Fe^{54})_{IRMM\text{-}014} - 1] \times 10^3$. Replicated measurements of CAGSR-1 (GBW-07105) yielded $\delta^{56}Fe$ of 0.13‰ ± 0.09‰ (2σ; n = 5), consistent with previously reported values (Craddock & Dauphas, 2011). Analytical results are given in Table S1 in Supporting Information S1.

4. Results

The bauxites and bauxitic clays (Al_2O_3 > 35% and 1.8 < Al_2O_3/SiO_2 < 2.6) we examined are composed mainly of Al-hydroxide (diaspore and boehmite), followed by kaolinite and illite, and a small amount of Fe minerals and detrital minerals (e.g., anatase and zircon) (Figures 5a and 5b). The clay rocks are composed of clay minerals such as kaolinite and illite, with Al-hydroxides and detrital minerals (Figure 5c). The iron ores and iron-rich clays are composed of Fe minerals (mainly hematite with a small amount of goethite or siderite) and clay minerals, with a small amount of automorphic quartzes and almost no detrital minerals (Figures 5d–5f). The significantly different mineralogical features between bauxite and Fe bed samples indicate different origins, that is, the former is of detrital depositional origin, while the latter is of chemical depositional origin.

The bauxites/bauxitic clays have Al_2O_3 contents of 52.6–79.6 wt. %, SiO_2 contents of 1.48–30.1 wt. %, and Fe_2O_3 contents of 0.46–2.22 wt. %. Clay rocks have relatively lower Al_2O_3 contents (34.1–42.3 wt. %), but relatively higher SiO_2 (39.5–45.1) and Fe_2O_3 (0.72–5.82 wt. %) contents. Iron ores/iron-rich clays have the lowest Al_2O_3 contents (2.45–31.4 wt. %), moderate SiO_2 contents (6.76–36 wt. %), and the highest Fe_2O_3 contents (16.7–79.1 wt. %). All samples we examined contain extremely low organic carbon content (C_{org} < 0.16 wt. %) (Table S1 in Supporting Information S1), indicating an oxic depositional/diagenetic condition (Bennett & Canfield, 2020). Redox-sensitive elements Mo, U, and V are a reliable proxy of redox conditions in the depositional/diagenetic environment (e.g., Tribovillard et al., 2006) with Mo/Al, U/Al, and V/Al values below 1, 5, and 23 (μg g^{-1}/wt. %) indicating oxic conditions. Higher ratios indicate anoxic to euxinic conditions (Bennett & Canfield, 2020). In this study, the Mo/Al (<1), U/Al (<3), and V/Al (<20 μg g^{-1}/wt. %) ratios of our samples were extremely low and had no or negative correlation with the Al_2O_3/Fe_2O_3 ratios (Figure S2 in Supporting Information S1), indicating an oxidative depositional/diagenetic environment.

The ratio of highly reactive Fe (Fe_{HR} = Fe_{Py} + Fe_{carb} + Fe_{ox} + Fe_{mag}) to total Fe (Fe_T) is also a reliable proxy of redox conditions (Scholz, 2018; Scholz, Beil, et al., 2019), with its values <0.22, 0.22–0.38, and >0.38 representing the oxic, possibly anoxic, and anoxic conditions, respectively (Poulton & Canfield, 2005). Most of our samples have Fe_{HR}/Fe_T ratios lower than 0.38, and among them, clay rocks have higher Fe_{HR}/Fe_T ratios (average 0.36) than bauxites/bauxitic clays (average 0.27) and iron-rich clay (LD3-11: 0.128) (Figure 6a). In addition, Fe_{HR}/Fe_T values are negatively correlated with Al_2O_3/Fe_2O_3 ratios (Figure 6a). These results are again consistent with the formation under oxic conditions.

Bauxite/bauxitic clay has a higher proportion of silicate-bound Fe (average Fe_{sil}/Fe_T = 0.725, where Fe_{sil} = Fe_T − Fe_{HR}) than clay rock (average 0.645) (Figure 6b). The $\delta^{56}Fe$ values of bauxites/bauxitic clays vary

from −0.17‰ to +1.15‰ ($n = 21$), whereas clay rocks (−0.09‰ to +0.35‰; $n = 4$) and iron ores/iron-rich clays (−0.13‰ to +0.16‰; $n = 12$) have a narrower range of δ^{56}Fe values.

5. Discussion

5.1. Fe Loss During Karst Bauxite Formation

Karst bauxite is a kind of Fe-depleted and Al-enriched sedimentary rock, and its mineralization process mainly includes three stages: (a) pedogenesis, were the parent rocks are intensity chemically weathered to form Al-rich soils in warm climates; (b) sedimentary transport, were Al-rich soils are eroded and transported toward the continental margin by runoff; and (c) subsequent deposition and diagenesis to form karst bauxites (Bárdossy, 1982; Yu et al., 2019). The depositional basement, that is, carbonate rock and/or shale, has long been regarded as the source rock of central Guizhou bauxite (Ling et al., 2017; Yu et al., 2019). Intensive chemical weathering of the parent rock of bauxite forms Al-rich soils, which are subsequently eroded and effluxed to the ocean by rivers as dissolved phases (include colloid: 1–200 nm), particles including SPM (>0.2 μm), or sand (>63 μm) (Gaillardet et al., 2003). The detrital minerals (e.g., zircon and anatase) in bauxites studied here, which have been retained after diagenesis, are predominantly small in size (0.2–5.0 μm) (Figures 5a and 5b). Diaspore, the primary economic mineral in karst bauxite, is commonly columnar or platy and 1–10 μm in size (Figures 5a–5d). These particles are consistent in size with SPM, suggesting that the precursor materials leading to karst bauxite formation were mainly transported as riverine SPM.

Bauxite ores have significantly high Al_2O_3 (average 70.1 wt. %) and extremely low Fe_2O_3 (average 1.02 wt. %) contents (Table S1 in Supporting Information S1 and references therein), significantly different from normal sediments/sedimentary rocks and NASC (Al_2O_3 and Fe_2O_3 contents of 16.9 and 5.65 wt. %, respectively; Gromet et al., 1984). This difference in geochemical composition implies that karst bauxite formation in central Guizhou had significant Fe loss but retained Al. Mass-change calculations for the sedimentary basement of central Guizhou bauxites (Loushanguan Group dolomite) suggest that Fe loss occurred during the leaching stage of pedogenesis, supporting this inference (Ling et al., 2019). In addition, karst bauxite samples from around the world have a negative correlation between Al_2O_3 (average: 61.9 wt. %) and Fe_2O_3 (average 4.42 wt. %) contents (Figure 7), suggesting that Fe loss is a common process during karst bauxite formation. We tested if Fe loss occurred and at what stage of bauxite mineralization by examining the Fe stable isotopes of our samples.

5.2. Iron Isotopic Evidence of Fe Loss

In terrestrial ecosystems, surface weathering under strongly oxidizing conditions has limited Fe isotope fractionation, with mean δ^{56}Fe in clastic rocks and sediments of 0‰ ± 0.2‰ (e.g., Beard et al., 2003). The low Fe bauxites we investigated show high δ^{56}Fe values (up to +1.15‰) (Figure 8). Two processes can lead to high δ^{56}Fe values, loss of dissolved Fe(II) that is relatively enriched in ^{54}Fe, or the net addition of a component enriched in ^{56}Fe (Thompson et al., 2007; Yamaguchi et al., 2007). Our data, showing an inverse relationship between Fe and Al, support dissolved Fe(II) loss during karst bauxite formation (Figure 7), leading to high δ^{56}Fe values.

Four major processes have been postulated to control the dissolution of Fe minerals in terrestrial ecosystems: (a) proton-promoted dissolution, (b) oxidative dissolution, (c) reductive dissolution, and (d) ligand-controlled dissolution (B. Wu et al., 2019 and reference therein). Experimental studies demonstrated that proton-promoted dissolution (process (a) causes no or only limited, Fe isotope fractionation (Brantley et al., 2004; Wiederhold et al., 2006). In contrast, oxidative dissolution (process 2) always caused the accumulation of heavy Fe isotopes in the leachates, leaving behind a rock with relatively light δ^{56}Fe values (B. Wu et al., 2019). Reductive dissolution (process 3) under anoxic conditions, with or without bacteria, can produce aqueous Fe(II) that has 0.5‰–4‰ lower δ^{56}Fe values than the Fe(III) in the initial material (e.g., Brantley et al., 2004; Butler et al., 2005; Chanda et al., 2021; Icopini et al., 2004). Inorganic ligand-controlled dissolution (process 4) causes minor depletion (~0.5‰) in δ^{56}Fe values of the solid phase, whereas biotic/organic ligand-controlled dissolutions can cause significant Fe isotope fractionation (~2.2‰) (Brantley et al., 2004; Kiczka et al., 2010; Wiederhold et al., 2006). The Fe isotope fractionation caused by biotic/organic ligand-controlled dissolution was also caused by reductive dissolution due to the depletion of oxygen through microbial respiration (Brantley et al., 2004). This implies that during the karst bauxite formation, reductive dissolution under anoxic conditions may be the primary control on Fe isotope fractionation.

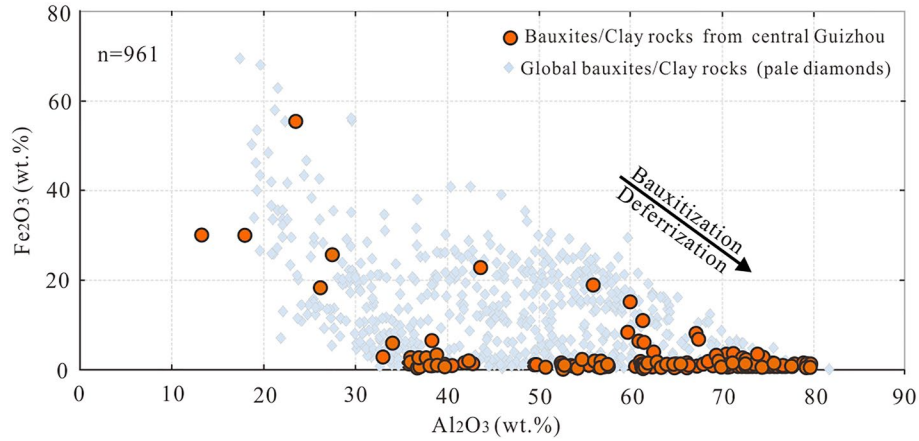

Figure 7. Al_2O_3 versus Fe_2O_3 diagrams for Carboniferous bauxite samples from central Guizhou (n = 172 samples), 130 of which are from Li (2013), Long et al. (2017), Ling et al. (2017, 2018), and Weng et al. (2019). Global data of karst bauxites from Mordberg et al. (2000), Mameli et al. (2007), Ye et al. (2008), Deng et al. (2010), Boni et al. (2012), Zarasvandi et al. (2012), Q. Wang et al. (2012), D. H. Wang et al. (2013), T. Wang et al. (2014), Hanilçi (2013), Z. Zhang et al. (2013), Li (2013), Z. H. Li et al. (2013), X. Liu et al. (2013, 2016), Abedini and Calagari (2014), Z. L. Huang et al. (2014), Mongelli et al. (2014), Yu et al. (2014, 2016), Zamanian et al. (2016), Hou et al. (2017), Khosravi et al. (2017), Long et al. (2017), Yuste et al. (2017), Abedini et al. (2018), Abedini, Khosravi and Dill (2020); Abedini, Mongelli et al. (2020), Weng et al. (2019), S. J. Yang et al. (2019, 2021), X. F. Liu et al. (2020), Ling et al. (2021), S. Q. Zhang et al. (2021), and Zhao et al. (2021).

5.3. Pedogenesis Leads to Fe Loss

Fe loss caused by reductive dissolution in the anoxic environment may have occurred at one or more stages of karst bauxite mineralization. The precursor materials leading to karst bauxite formation were mainly transported as riverine SPM. In the Phanerozoic with an oxidizing atmosphere, the presence of abundant O_2 in river water prevented the reductive dissolution of Fe from taking place (Canfield, 1997). This ruled out the possibility that Fe loss occurred in the sedimentary transport stage.

Continental marginal sediments may have released dissolved Fe during depositional/diagenetic processes (Dale et al., 2015; Elrod et al., 2004; John et al., 2012; Lam & Bishop, 2008; Noffke et al., 2012; Scholz et al., 2014; Scholz, Schmidt, et al., 2019; Severmann et al., 2010). However, published marginal sediments have δ^{56}Fe values ranging from −0.32‰ to +0.3‰ (B. Wu et al., 2019 and reference therein). The less heterogeneous δ^{56}Fe values relative to bauxite ores suggest that the depositional/diagenetic process was unlikely to be the controlling factor in the dissolved Fe released. This is consistent with the C_{org}, Fe species, and redox-sensitive element studies, the results all of which suggest that the bauxites in central Guizhou were formed under oxic depositional/diagenetic conditions (Table S1 in Supporting Information S1; Figure 6 and Figure S2 in Supporting Information S1). Consequently, we hypothesize that most of the Fe loss occurred during the pedogenic stage of karst bauxite formation under anoxic conditions.

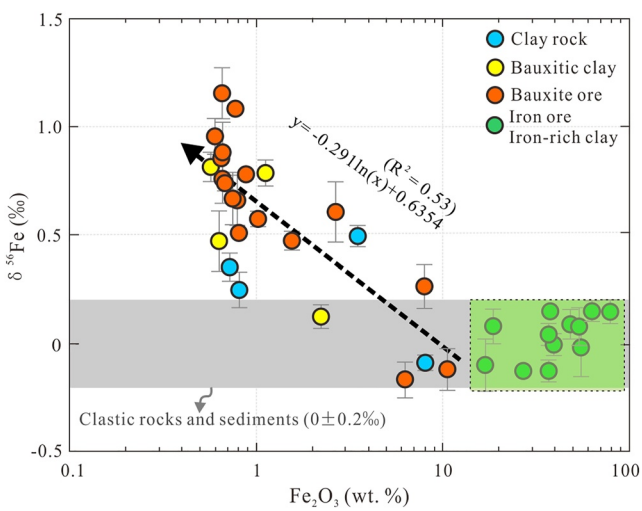

Figure 8. δ^{56}Fe versus Fe_2O_3 diagram. The average δ^{56}Fe value of normal clastic rocks and sediments is obtained from Beard et al. (2003).

The pedogenic process can develop a relatively wide range of δ^{56}Fe values (−0.52‰ to +1.04‰) compared with their parent rocks during primary dissolution and secondary processes, such as oxidation, precipitation, as well as complexation with soil organic matter (Fekiacova et al., 2013, 2017; Garnier et al., 2017; Johnson et al., 2008; Kiczka et al., 2011; S. Liu et al., 2014; Qi et al., 2022; Thompson et al., 2007; Yesavage et al., 2012). When anoxic conditions are present in water-saturated soil with high rainfall, the Fe isotope fractionation during weathering is redox-controlled and can show elevated δ^{56}Fe values due to a preferential release of light Fe isotopes (Akerman et al., 2014; S. Liu et al., 2014; Schuth et al., 2015; Thompson et al., 2007; Wiederhold et al., 2007a; Yamaguchi et al., 2007). For instance,

the soil horizon in Hawaiian, studied by Thompson et al. (2007), exhibited high δ^{56}Fe values (up to +0.72‰) due to increased Fe loss in the soil profile under enhanced anoxic conditions. Another example is the Paleoproterozoic Hekpoort paleosol profile from Gaborone, Botswana (~2.2 Ga), that has high δ^{56}Fe values (−0.17‰ to +1.04‰ with an average of +0.55‰) and negative correlation between δ^{56}Fe ratios and Fe_2O_3 contents. These paleosols are considered to be a result of Fe(II) loss under reduced, organic-acid bearing soil water and groundwater (Yamaguchi et al., 2007). Our data showing increasing bulk δ^{56}Fe values in conjunction with the logarithmic decrease in Fe_2O_3 content (R^2 = 0.53) in bauxite samples (Figure 8), is consistent with the residual Fe-depleted soil being enriched in heavy Fe isotopes due to preferential removal of light Fe isotopes during pedogenesis under anoxic conditions.

In addition to bauxites having the highest δ^{56}Fe values (up to +1.15‰) and Fe_{sil}/Fe_T ratios (average: 0.725), the positive correlation between Al_2O_3/Fe_2O_3 and Fe_{sil}/Fe_T ratios (Figure 6b) indicates that the Fe species in the bauxite ore is controlled by Fe_{sil} with elevated δ^{56}Fe values that were inherited from Fe-depleted soils. This is consistent with the δ^{56}Fe values of the Fe_{Sil} fractions (up to +1.5‰) published to date that are exclusively positive Fe species in soils (B. Wu et al., 2019 and reference therein). Therefore, it is reasonable to hypothesize that during pedogenesis, dissolved Fe(II) with light Fe isotopes were preferentially removed from the primary minerals during continental weathering, leaving the Fe_{sil} in residual soil with heavy Fe isotopic fingerprints (Fekiacova et al., 2013; B. Wu et al., 2019). However, most of this dissolved Fe(II) may have been rapidly re-oxidized to Fe(III) prior to its migration, likely as colloidal substances (M. Li et al., 2017; B. Wu et al., 2019). This oxidation process produces Fe(III) with δ^{56}Fe values 0.5‰–4‰ higher than that of Fe(II) in the initial material, as observed in both laboratory experiments (Anbar et al., 2005; Beard et al., 2010; Johnson et al., 2002; Nie et al., 2017; L. Wu et al., 2012) and field studies (M. Li et al., 2017; Wiederhold et al., 2007b; R. Zhang et al., 2015). The Fe(III) colloids could have Fe isotopic compositions similar to that of continental crust (δ^{56}Fe = +0.07‰) due to their similar extent of isotopic fractionation between the oxidation of Fe(II) to Fe(III) and the reduction of Fe(III) to Fe(II) (M. Li et al., 2017; Poitrasson et al., 2008; Wiederhold et al., 2006; B. Wu et al., 2019; R. Zhang et al., 2015). Such reductive dissolution and re-oxidation has been widely observed during pedogenesis (L. M. Huang et al., 2018; M. Li et al., 2017; Schuth et al., 2015; Thompson et al., 2007; Wiederhold et al., 2007b).

5.4. Genesis of Iron Beds Beneath Bauxite Beds

The results of petrological and mineralogical studies suggest that iron ore/iron-rich clay was precipitated through a chemical process, that is, Fe(III) colloid precipitated directly due to flocculation or formation of insoluble Fe(III) due to oxidation of dissolved Fe(II) in the water column (Figures 4 and 5, Boyle et al., 1977). River input was the most likely Fe source for these iron ore/iron-rich clay deposits in the continental margin (Escoube et al., 2009; W. Li et al., 2015). In the Phanerozoic era, however, riverine dissolved Fe is dominated by Fe(III) colloids and rare dissolved Fe(II) (Boyle et al., 1977; Johnson et al., 2002; B. Wu et al., 2019). Therefore, a possible mechanism for the formation of iron beds would be the precipitation of riverine Fe(III) colloids prior to the deposition of bauxite beds in the central Guizhou region. Iron bed samples (−0.13‰ to +0.16‰) show similar Fe isotopic compositions to riverine Fe(III) colloids and continental crust (Figure 8, Fantle & DePaolo, 2004; Ingri et al., 2006), further supporting this interpretation.

Overall, our results support a Fe release and reprecipitation processes during karst bauxite formation in central Guizhou, southwestern China as follows (Figure 9): (a) during the early Carboniferous period, intensive continental weathering under a greenhouse climate may have enhanced the release of isotopically light Fe(II) through reductive dissolution under anoxic conditions in water-saturated soils, leaving the silicate bound Fe in residual soils with heavy Fe isotopic fingerprints; (b) the majority of these dissolve Fe(II) were rapidly oxidized in the presence of O_2 to Fe(III) with a δ^{56}Fe value around zero, and were transported in colloidal form by rivers to the continental margin, forming thin Fe-bed layers in karst depressions via chemical precipitation; (c) the Fe-depleted and Al-enriched soils were then transported as riverine SPM and deposited upon the iron bed forming karst bauxite bed that inherits the Fe isotopic composition of soils.

6. Conclusions and Implications

The high Al_2O_3 and low Fe_2O_3 contents of the studied bauxite samples indicate Fe loss during Carboniferous karst bauxite formation in central Guizhou, southwestern China. The relatively high bauxite δ^{56}Fe values

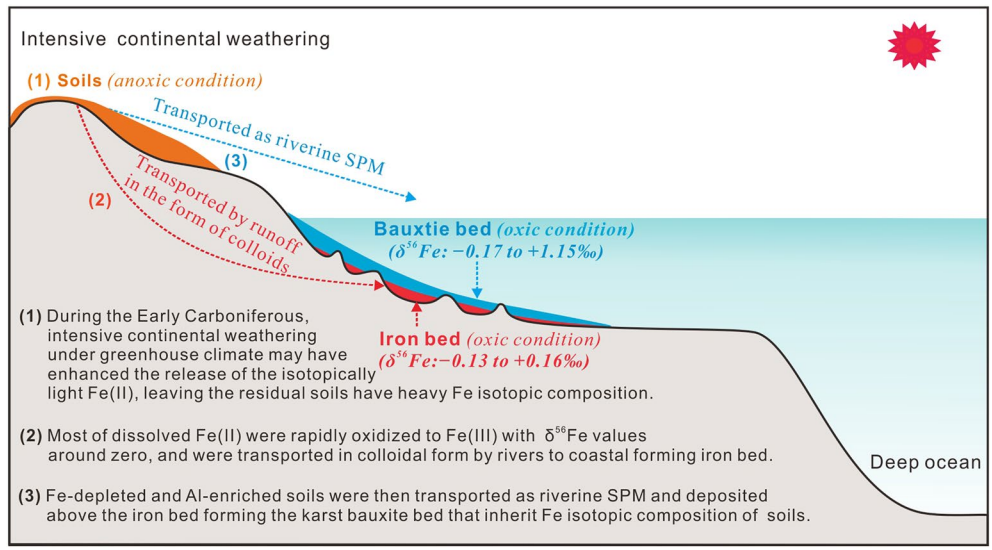

Figure 9. A conceptual model to account for the Early Carboniferous bauxite formation in central Guizhou, SW China.

(−0.17‰ ± 0.09–1.15‰ ± 0.13‰, average 0.58‰ ± 0.09‰) but low C_{org} contents and low Fe_{HR}/Fe_T, Mo/Al, U/Al, and V/Al ratios suggest oxic diagenetic but anoxic pedogenic conditions during karst bauxite formation. The increasing bulk $\delta^{56}Fe$ values with a decrease in logarithmic Fe_2O_3 concentrations of bauxites indicate that the incomplete reduction of Fe(III) during pedogenesis releases isotopically light dissolved Fe(II), leaving heavier Fe in the residual soils to eventually be recorded in bauxites. Most of the dissolved Fe(II) were rapidly oxidized to Fe(III) with $\delta^{56}Fe$ values around zero and transported toward the paleo-continental margin of the western South China Plate, forming Fe ore and Fe-rich clay with $\delta^{56}Fe$ values of −0.13‰ to +0.16‰) via chemical deposition. Subsequently, Fe-depleted and Al-enriched soils were transported (mainly as riverine SPM) to the continental margin forming bauxite beds overlying Fe beds.

This study documents the release of Fe into the ocean during the pedogenic stage of the bauxite mineralization in the early Carboniferous period. The deposition of Fe beds prior to bauxite beds in central Guizhou further strengthens our interpretation. The negative correlation between Al_2O_3 and Fe_2O_3 in global karst bauxites suggests that Fe loss during karst bauxite formation was a common effect and that the karst bauxite could act as a reliable indicator of additional Fe to the ocean during continental weathering. Humid climate periods of extensive karst bauxite formation would have been characterized by an additional efflux of Fe to the ocean, particularly during the Carboniferous, Permian, Cretaceous periods, and Cenozoic eras. This additional Fe supply may have had a critical impact on the oceanic Fe cycle and marine ecosystems in the early Carboniferous period.

Conflict of Interest

The authors declare no conflicts of interest relevant to this study.

Acknowledgments
This work was supported by the National Natural Science Foundation of China (Grants 92062107, U1812402, and 92162214), the Guizhou Provincial Science and Technology Projects (Grant ZK[2021]046), the Key Research Program of the Chinese Academy of Sciences (Grant ZDRW-ZS-2020-4-1), and the Key Research Program of the Institute of Geology & Geophysics, CAS (Grant IGGCAS-201902). The authors would like to thank Prof. Runsheng Yin for his valuable advice, and Prof. Chao Li and Prof. Zihu Zhang for their help with the Fe species extraction experiment.

Data Availability Statement

All geochemical data are accessible in the Figshare data repositories: the geochemical and iron isotope data are available as Ling (2022) and geochemical data used in Figure 7 are available as Ling (2023).

References

Abedini, A., & Calagari, A. A. (2014). REE geochemical characteristics of titanium-rich bauxites: The Permian Kanigorgeh horizon, NW Iran. *Turkish Journal of Earth Sciences*, *23*, 513–532. https://doi.org/10.3906/yer-1404-11

Abedini, A., Habibi Mehr, M., Khosravi, M., & Calagari, A. A. (2019). Geochemical characteristics of the karst-type bauxites: An example from the Kanirash deposit, NW Iran. *Arabian Journal of Geosciences*, *12*(15), 1–16. https://doi.org/10.1007/s12517-019-4601-z

Abedini, A., Khosravi, M., & Calagari, A. A. (2018). Geochemical characteristics of the Arbanos karst-type bauxite deposit, NW Iran: Implications for parental affinity and factors controlling the distribution of elements. *Journal of Geochemical Exploration*, *200*, 249–265. https://doi.org/10.1016/j.gexplo.2018.09.004

Abedini, A., Khosravi, M., & Dill, H. G. (2020). Rare Earth element geochemical characteristics of the late Permian Badamlu karst bauxite deposit, NW Iran. *Journal of African Earth Sciences*, *172*, 103974. https://doi.org/10.1016/j.jafrearsci.2020.103974

Abedini, A., Khosravi, M., & Mongelli, G. (2022a). Geochemistry of the early Jurassic Soleiman Kandi karst bauxite deposit, Irano-Himalayan belt, NW Iran: Constraints on bauxite Genesis and the distribution of critical raw materials. *Journal of Geochemical Exploration*, *241*, 107056. https://doi.org/10.1016/j.gexplo.2022.107056

Abedini, A., Khosravi, M., & Mongelli, G. (2022b). The middle Permian pyrophyllite-rich ferruginous bauxite, northwestern Iran, Irano-Himalayan karst belt: Constraints on elemental fractionation and provenance. *Journal of Geochemical Exploration*, *233*, 106905. https://doi.org/10.1016/j.gexplo.2021.10690

Abedini, A., Mongelli, G., Khosravi, M., & Sinisi, R. (2020). Geochemistry and secular trends in the middle–late Permian karst bauxite deposits, northwestern Iran. *Ore Geology Reviews*, *124*, 103660. https://doi.org/10.1016/j.oregeorev.2020.103660

Abedini, A., Rezaei Azizi, M., & Calagari, A. A. (2019a). REE mobility and tetrad effects bauxites: An example from the Kanisheeteh deposit, NW Iran. *Acta Geodynamica et Geomaterialia*, *193*, 11–26. https://doi.org/10.13168/agg.2019.0002

Abedini, A., Rezaei Azizi, M., & Calagari, A. A. (2019b). REE tetrad effect as a powerful indicator of formation conditions of karst bauxites: A case study of the Shahindezh deposit, NW Iran. *Acta Geologica Sinica*, *93*(4), 912–927. https://doi.org/10.1111/1755-6724.13763

Akerman, A., Poitrasson, F., Oliva, P., Audry, S., Prunier, J., & Braun, J. (2014). The isotopic fingerprint of Fe cycling in an equatorial soil–plant–water system: The Nsimi watershed, South Cameroon. *Chemical Geology*, *385*, 104–116. https://doi.org/10.1016/j.chemgeo.2014.07.003

Anbar, A. D., Jarzecki, A. A., & Spiro, T. G. (2005). Theoretical investigation of iron isotope fractionation between $Fe(H_2O)^{63+}$ and $Fe(H_2O)^{62+}$: Implications for iron stable isotope geochemistry. *Geochimica et Cosmochimica Acta*, *69*(4), 825–837. https://doi.org/10.1016/j.gca.2004.06.012

Bárdossy, G. (1982). *Karst bauxites, bauxite deposits on carbonate rocks*. Developments in economic geology (Vol. 14). Elsevier. https://doi.org/10.1016/0016-7061(83)90006-x

Beard, B. L., Handler, R. M., Scherer, M. M., Wu, L., Czaja, A. D., Heimann, A., & Johnson, C. M. (2010). Iron isotope fractionation between aqueous ferrous iron and goethite. *Earth and Planetary Science Letters*, *295*(1–2), 241–250. https://doi.org/10.1016/j.epsl.2010.04.006

Beard, B. L., Johnson, C. M., Von Damm, K. L., & Poulson, R. L. (2003). Iron isotope constraints on Fe cycling and mass balance in oxygenated Earth oceans. *Geology*, *31*(7), 629–632. https://doi.org/10.1130/0091-7613(2003)031<0629:iicofc>2.0.co;2

Bennett, W. W., & Canfield, D. E. (2020). Redox-sensitive trace metals as paleoredox proxies: A review and analysis of data from modern sediments. *Earth-Science Reviews*, *204*, 103175. https://doi.org/10.1016/j.earscirev.2020.103175

Bergquist, B. A., & Boyle, E. A. (2006). Iron isotopes in the Amazon River system: Weathering and transport signatures. *Earth and Planetary Science Letters*, *248*(1–2), 54–68. https://doi.org/10.1016/j.epsl.2006.05.004

Bogatyrev, B. A., Zhukov, V. V., & Tsekhovsky, Y. G. (2009). Phanerozic bauxite epochs. *Geology of Ore Deposits*, *51*(6), 456–466. https://doi.org/10.1134/S1075701509060038

Boni, M., Reddy, S. M., Mondillo, N., Balassone, G., & Taylor, R. (2012). A distant magmatic source for Cretaceous karst bauxites of southern Apennines (Italy), revealed through SHRIMP zircon age dating. *Terra Nova*, *24*(4), 326–332. https://doi.org/10.1111/j.1365-3121.2012.01068.x

Boyd, P. W., & Ellwood, M. J. (2010). The biogeochemical cycle of iron in the ocean. *Nature Geoscience*, *3*(10), 675–682. https://doi.org/10.1038/ngeo964

Boyle, E. A., Edmond, J. M., & Sholkovitz, E. R. (1977). The mechanism of iron removal in estuaries. *Geochimica et Cosmochimica Acta*, *41*(9), 1313–1324. https://doi.org/10.1016/0016-7037(77)90075-8

Brantley, S. L., Liermann, L. J., Guynn, R. L., Anbar, A., Icopini, G. A., & Barling, J. (2004). Fe isotopic fractionation during mineral dissolution with and without bacteria. *Geochimica et Cosmochimica Acta*, *68*(15), 3189–3204. https://doi.org/10.1016/j.gca.2004.01.023

Butler, I. B., Archer, C., Vance, D., Oldroyd, A., & Rickard, D. (2005). Fe isotope fractionation of FeS formation in ambient aqueous solution. *Earth and Planetary Science Letters*, *236*(1–2), 430–442. https://doi.org/10.1016/j.epsl.2005.05.022

Calagari, A. A., & Abedini, A. (2007). Geochemical investigations on Permo-Triassic bauxite horizon at Kanisheeteh, east of Bukan, west-Azarbaidjan, Iran. *Journal of Geochemical Exploration*, *94*(1–3), 1–18. https://doi.org/10.1016/j.gexplo.2007.04.003

Canfield, D. E. (1997). The geochemistry of river particulates from the continental USA: Major elements. *Geochimica et Cosmochimica Acta*, *61*(16), 3349–3365. https://doi.org/10.1016/S0016-7037(97)00172-5

Canfield, D. E., Raiswell, R., Westrich, J. T., Reaves, C. M., & Berner, R. A. (1986). The use of chromium reduction in the analysis of reduced inorganic sulfur in sediments and shales. *Chemical Geology*, *54*(1–2), 149–155. https://doi.org/10.1016/0009-2541(86)90078-1

Chanda, P., Amenabar, M. J., Boyd, E. S., Beard, B. L., & Johnson, C. M. (2021). Stable Fe isotope fractionation during dissimilatory Fe(III) reduction by a thermoacidophile in acidic hydrothermal environment. *Geochimica et Cosmochimica Acta*, *292*, 427–251. https://doi.org/10.1016/j.gca.2020.09.025

Chen, T. Y., Li, W. Q., Guo, B., Liu, R. L., Li, G. J., Zhao, L., & Ji, J. F. (2020). Reactive iron isotope signatures of the east Asian dust particles: Implications for iron cycling in the deep North Pacific. *Chemical Geology*, *531*, 119342. https://doi.org/10.1016/j.chemgeo.2019.119342

Craddock, P. R., & Dauphas, N. (2011). Iron isotopic compositions of geological reference materials and chondrites. *Geostandards and Geoanalytical Research*, *35*(1), 101–123. https://doi.org/10.1111/j.1751-908x.2010.00085.x

Dale, A. W., Nickelsen, L., Scholz, F., Hensen, C., Oschlies, A., & Wallmann, K. (2015). A revised global estimate of dissolved iron fluxes from marine sediments. *Global Biogeochemical Cycles*, *29*(5), 691–707. https://doi.org/10.1002/2014gb005017

Deng, J., Wang, Q. F., Yang, S. J., Liu, X. F., Zhang, Q. Z., Yang, L. Q., & Yang, Y. H. (2010). Genetic relationship between the Emeishan plume and the bauxite deposits in western Guangxi, China: Constraints from U–Pb and Lu–Hf isotopes of the detrital zircons in bauxite ores. *Journal of Asian Earth Sciences*, *37*(5–6), 412–424. https://doi.org/10.1016/j.jseaes.2009.10.005

Elrod, V. A., Berelson, W. M., Coale, K. H., & Johnson, K. S. (2004). The flux of iron from continental shelf sediments: A missing source for global budgets. *Geophysical Research Letters*, *31*(12), L12307. https://doi.org/10.1029/2004gl020216

Escoube, R., Rouxel, O. J., Sholkovitz, E., & Donard, O. F. X. (2009). Iron isotope systematics in estuaries: The case of North River, Massachusetts (USA). *Geochimica et Cosmochimica Acta*, *73*(14), 4045–4059. https://doi.org/10.1016/j.gca.2009.04.026

Fantle, M. S., & DePaolo, D. J. (2004). Iron isotopic fractionation during continental weathering. *Earth and Planetary Science Letters*, *228*(3), 547–562. https://doi.org/10.1016/j.epsl.2004.10.013

Fekiacova, Z., Pichat, S., Cornu, S., & Balesdent, J. (2013). Inferences from the vertical distribution of Fe isotopic compositions on pedogenetic processes in soils. *Geoderma*, *209*, 110–118. https://doi.org/10.1016/j.geoderma.2013.06.007

Fekiacova, Z., Vermeire, M. L., Bechon, L., Cornelis, J. T., & Cornu, S. (2017). Can Fe isotope fractionations trace the pedogenetic mechanisms involved in podolization? *Geoderma*, *296*, 38–46. https://doi.org/10.1016/J.GEODERMA.2017.02.020

Gaillardet, J., Viers, J., & Dupré, B. (2003). Trace element in river waters. Treatise on geochemistry. In J. I. Drever, H. D. Holland, & K. K. Turekian (Eds.), *Surface and ground water, weathering, erosion and soils* (Vol. 5). Pergamon. https://doi.org/10.1016/B0-08-043751-6/05165-3

Garnier, J., Garnier, J. M., Vieira, C. L., Akerman, A., Chmeleff, J., Ruiz, R. I., & Poitrasson, F. (2017). Iron isotope fingerprints of redox and biogeochemical cycling in the soil-water rice plant system of a paddy field. *Science of the Total Environment*, *574*, 1622–1632. https://doi.org/10.1016/j.scitotenv.2016.08.202

Gromet, L. P., Dymek, R. F., Haskin, L. A., & Korotev, R. L. (1984). The "North American shale composite": Its compilation, major and trace element characteristics. *Geochimica et Cosmochimica Acta*, *48*(12), 2469–2482. https://doi.org/10.1016/0016-7037(84)90298-9

Hanilçi, N. (2013). Geological and geochemical evolution of the Bolkardaği bauxite deposits, Karaman, Turkey: Transformation from shale to bauxite. *Journal of Geochemical Exploration*, *133*, 118–137. https://doi.org/10.1016/j.gexplo.2013.04.004

Hou, Y. L., Zhong, Y. T., Xu, Y. G., & He, B. (2017). The provenance of late Permian karstic bauxite deposits in SW China, constrained by the geochemistry of interbedded clastic rocks, and U–Pb–Hf–O isotopes of detrital zircons. *Lithos*, *278–281*, 240–254. https://doi.org/10.1016/j.lithos.2017.01.013

Huang, L. M., Jia, X. X., Zhang, G. L., Thompson, A., Huang, F., Shao, M. A., & Cheng, L. M. (2018). Variations and controls of iron oxides and isotope compositions during paddy soil evolution over a millennial time scale. *Chemical Geology*, *476*, 340–351. https://doi.org/10.1016/j.chemgeo.2017.11.030

Huang, Z. L., Jin, Z. G., Xiang, X. L., Gu, J., Wu, G. H., Chen, X. L., et al. (2014). *Metallogenic theory and prediction of bauxite deposits in the Wuchuan-Zheng'an-Daozhen area, Northern Guizhou Province, China* (pp. 1–245). Science Press.

Icopini, G. A., Anbar, A. D., Ruebush, S. S., Tien, M., & Brantley, S. L. (2004). Iron isotope fractionation during microbial reduction of iron: The importance of adsorption. *Geology*, *32*(3), 205–208. https://doi.org/10.1130/G20184.1

Ilina, S. M., Poitrasson, F., Lapitskiy, S. A., Alekhin, Y. V., Viers, J., & Pokrovsky, O. S. (2013). Extreme iron isotope fractionation between colloids and particles of boreal and temperate organic-rich waters. *Geochimica et Cosmochimica Acta*, *101*, 96–111. https://doi.org/10.1016/j.gca.2012.10.023

Ingri, J., Malinovsky, D., Rodushkin, I., Baxter, D. C., Widerlund, A., Andersson, P., et al. (2006). Iron isotope fractionation in river colloidal matter. *Earth and Planetary Science Letters*, *245*(3–4), 792–798. https://doi.org/10.1016/j.epsl.2006.03.031

Jickells, T. D., An, Z. S., Andersen, K. K., Baker, A. R., Brooks, N., Cao, J. J., et al. (2005). Global iron connections between desert dust, ocean biogeochemistry, and climate. *Science*, *308*(5718), 67–71. https://doi.org/10.1126/science.110595

John, S. G., Mendez, J., Moffett, J. W., & Adkins, J. F. (2012). The flux of iron and iron isotopes from San Pedro Basin sediments. *Geochimica et Cosmochimica Acta*, *93*, 14–29. https://doi.org/10.1016/j.gca.2012.06.003

Johnson, C. M., Beard, B. L., & Roden, E. E. (2008). The iron isotope fingerprints of redox and biogeochemical cycling in modern and ancient Earth. *Annual Review of Earth and Planetary Sciences*, *36*(1), 457–493. https://doi.org/10.1146/annurev.earth.36.031207.124139

Johnson, C. M., Skulan, J. L., Beard, B. L., Sun, H., Nealson, K. H., & Braterman, P. S. (2002). Isotopic fractionation between Fe (III) and Fe (II) in aqueous solutions. *Earth and Planetary Science Letters*, *195*(1), 141–153. https://doi.org/10.1016/S0012-821X(01)00581-7

Kalaitzidis, S., Siavalas, G., Skarpelis, N., Araujo, C. V., & Christanis, K. (2010). Late Cretaceous coal overlying karstic bauxite deposits in the Parnassus-Ghiona unit, central Greece: Coal characteristics and depositional environment. *International Journal of Coal Geology*, *81*(4), 211–226. https://doi.org/10.1016/j.coal.2009.06.005

Khosravi, M., Abedini, A., Alipour, S., & Mongelli, G. (2017). The Darzi-Vali bauxite deposit, West-Azarbaidjan Province, Iran: Critical metals distribution and parental affinities. *Journal of African Earth Sciences*, *129*, 960–972. https://doi.org/10.1016/j.jafrearsci.2017.02.024

Khosravi, M., Vérard, C., & Abedini, A. (2021). Palaeogeographic and geodynamic control on the Iranian karst-type bauxite deposits. *Ore Geology Reviews*, *139*, 104589. https://doi.org/10.1016/j.oregeorev.2021.104589

Kiczka, M., Wiederhold, J. G., Frommer, J., Kraemer, S. M., Bourdon, B., & Kretzschmar, R. (2010). Iron isotope fractionation during proton- and ligand-promoted dissolution of primary phyllosilicates. *Geochimica et Cosmochimica Acta*, *74*(11), 3112–3128. https://doi.org/10.1016/j.gca.2010.02.018

Kiczka, M., Wiederhold, J. G., Frommer, J., Voegelin, A., Kraemer, S. M., Bourdon, B., & Kretzschmar, R. (2011). Iron speciation and isotope fractionation during silicate weathering and soil formation in an alpine glacier forefield chronosequence. *Geochimica et Cosmochimica Acta*, *75*(19), 5559–5573. https://doi.org/10.1016/j.gca.2011.07.008

Lam, P. J., & Bishop, J. K. B. (2008). The continental margin is a key source of iron to the HNLC North Pacific Ocean. *Geophysical Research Letters*, *35*(7), 521–539. https://doi.org/10.1029/2008gl033294

Li, M., He, Y. S., Kang, J. T., Yang, X. Y., He, Z. W., Yu, H. M., & Huang, F. (2017). Why was iron lost without significant isotope fractionation during the lateritic process in tropical environments? *Geoderma*, *290*, 1–9. https://doi.org/10.1016/j.geoderma.2016.12.003

Li, W., Beard, B. L., & Johnson, C. M. (2015). Biologically recycled continental iron is a major component in banded iron formations. *Proceedings of the National Academy of Sciences of the United States of America*, *112*(27), 8193–8198. https://doi.org/10.1073/pnas.1505515112

Li, Y. J. (2013). *Analysis of geochemical characteristics and genesis of bauxite in Guizhou* (pp. 1–82). The Master Dissertation of University of Chinese Academy of Sciences.

Li, Z. H., Din, J., Xu, J. S., Liao, C. G., Yin, F. G., Lv, T., et al. (2013). Discovery of the REE minerals in the Wulong–Nanchuan bauxite deposits, Chongqing, China: Insights on conditions of formation and processes. *Journal of Geochemical Exploration*, *133*, 88–102. https://doi.org/10.1016/j.gexplo.2013.06.016

Ling, K. Y. (2022). Geochemical data of karst bauxite in Southwest China (Version 11) [Dataset]. Figshare. https://doi.org/10.6084/m9.figshare.21225947.v11

Ling, K. Y. (2023). Al_2O_3 and Fe_2O_3 content of bauxite samples (Version 9) [Dataset]. Figshare. https://doi.org/10.6084/m9.figshare.22187854.v9

Ling, K. Y., Wen, H. J., Zhang, Q. Z., Luo, C. G., Gu, H. N., Du, S. J., & Yu, W. X. (2021). Super-enrichment of lithium and niobium in the upper Permian Heshan Formation in Pingguo, Guangxi, China. *Science China Earth Sciences*, *64*(5), 753–772. https://doi.org/10.1007/s11430-020-9752-6

Ling, K. Y., Wen, H. J., Zhang, Z. W., Zhu, X. Q., & Tang, H. S. (2019). Geochemical characteristics of dolomite weathering profiles and revelations to enrichment mechanism of trace elements in the Jiujialu Formation, central Guizhou Province. *Acta Petrologica Sinica*, *35*(11), 3385–3397. https://doi.org/10.18654/1000-0569/2019/11.08

Ling, K. Y., Zhu, X. Q., Tang, H. S., Du, S. J., & Gu, J. (2018). Geology and geochemistry of the Xiaoshanba bauxite deposit, Central Guizhou Province, SW China: Implications for the behavior of trace and rare Earth elements. *Journal of Geochemical Exploration*, *190*, 170–186. https://doi.org/10.1016/j.gexplo.2018.03.007

Ling, K. Y., Zhu, X. Q., Tang, H. S., & Li, S. X. (2017). Importance of hydrogeological conditions during formation of the karstic bauxite deposits, Central Guizhou Province, Southwest China: A case study at Lindai deposit. *Ore Geology Reviews*, *82*, 198–216. https://doi.org/10.1016/j.oregeorev.2016.11.033

Liu, S., Teng, F., Li, S., Wei, G., Ma, J., & Li, D. (2014). Copper and iron isotope fractionation during weathering and pedogenesis: Insights from saprolite profiles. *Geochimica et Cosmochimica Acta*, *146*, 59–75. https://doi.org/10.1016/j.gca.2014.09.040

Liu, X., Wang, Q., Feng, Y., Li, Z. M., & Cai, S. (2013). Genesis of the Guangou karstic bauxite deposit in western Henan, China. *Ore Geology Reviews*, *55*, 162–175. https://doi.org/10.1016/j.oregeorev.2013.06.002

Liu, X., Wang, Q., Zhang, Q., Yang, S., Liang, Y., Zhang, Y., et al. (2017). Genesis of the Permian karstic Pingguo bauxite deposit, western Guangxi, China. *Mineralium Deposita*, *52*(7), 1031–1048. https://doi.org/10.1007/s00126-017-0723-y

Liu, X., Wang, Q., Zhang, Q., Zhang, Y., & Li, Y. (2016). Genesis of REE minerals in the karstic bauxite in western Guangxi, China, and its constraints on the deposit formation conditions. *Ore Geology Reviews*, *75*, 100–115. https://doi.org/10.1016/j.oregeorev.2015.12.015

Liu, X. F., Wang, Q. F., Zhao, L. H., Peng, Y. B., Ma, Y., & Zhou, Z. H. (2020). Metallogeny of the large-scale Carboniferous karstic bauxite in the Sanmenxia area, southern part of the North China Craton, China. *Chemical Geology*, *556*, 119851. https://doi.org/10.1016/j.chemgeo.2020.119851

Liu, X. M., Rudnick, R. L., McDonough, W. F., & Cummings, M. L. (2013). Influence of chemical weathering on the composition of the continental crust: Insights from Li and Nd isotopes in bauxite profiles developed on Columbia River Basalts. *Geochimica et Cosmochimica Acta*, *115*, 73–91. https://doi.org/10.1016/j.gca.2013.03.043

Long, Y. Z., Chi, G. X., Liu, J. P., Jin, Z. G., & Dai, T. G. (2017). Trace and rare Earth elements constraints on the sources of the Yunfeng paleo-karstic bauxite deposit in the Xiuwen-Qingzhen area, Guizhou. China. *Ore Geology Reviews*, *91*, 404–418. https://doi.org/10.1016/j.oregeorev.2017.09.014

Ma, J. L., Wei, G. J., Xu, Y. G., Long, W. G., & Sun, W. D. (2007). Mobilization and redistribution of major and trace elements during extreme weathering of basalt in Hainan Island. South China. *Geochimica et Cosmochimica Acta*, *71*(13), 3223–3237. https://doi.org/10.1016/j.gca.2007.03.035

Ma, Y. S., Chen, H. D., Wang, G. L., Guo, T. L., Tian, J. C., Liu, W. J., et al. (2009). *Sequence stratigraphy and paleogeography in South China* (pp. 1–603). China Science Publishing.

Mameli, P., Mongelli, G., Oggiano, G., & Dinelli, E. (2007). Geological, geochemical and mineralogical features of some bauxite deposits from Nurra (western Sardinia, Italy): Insights on conditions of formation and parental affinity. *International Journal of Earth Sciences*, *96*(5), 887–902. (Geologische Rundschau). https://doi.org/10.1007/s00531-006-0142-2

Metcalfe, I. (2006). Palaeozoic and mesozoic tectonic evolution and palaeogeography of east Asian crustal fragments: The Korean Peninsula in context. *Gondwana Research*, *9*(1–2), 24–46. https://doi.org/10.1016/j.gr.2005.04.002

Mongelli, G., Boni, M., Buccione, R., & Sinisi, R. (2014). Geochemistry of the Apulian karst bauxites (southern Italy): Chemical fractionation and parental affinities. *Ore Geology Reviews*, *63*, 9–21. https://doi.org/10.1016/j.oregeorev.2014.04.012

Mordberg, L. E., Stanley, C. J., & Germann, K. (2000). Rare Earth element anomalies in crandallite group minerals from the Schugorsk bauxite deposit, Timan, Russia. *European Journal of Mineralogy*, *12*(6), 1229–1243. https://doi.org/10.1127/0935-1221/2000/0012-1229

Nie, N. X., Dauphas, N., & Greenwood, R. C. (2017). Iron and oxygen isotope fractionation during iron UV photo-oxidation: Implications for early Earth and Mars. *Earth and Planetary Science Letters*, *458*, 179–191. https://doi.org/10.1016/j.epsl.2016.10.035

Noffke, A., Hensen, C., Sommer, S., Scholz, F., Bohlem, L., Mosch, T., et al. (2012). Benthic iron and phosphorus fluxes across the Peruvian oxygen minimum zone. *Limnology & Oceanography*, *57*(3), 851–867. https://doi.org/10.4319/lo.2012.57.3.0851

Pistiner, J. S., & Henderson, G. M. (2003). Lithium-isotope fractionation during continental weathering processes. *Earth and Planetary Science Letters*, *214*(1–2), 327–339. https://doi.org/10.1016/S0012-821X(03)00348-0

Poitrasson, F., Viers, J., Martin, F., & Braun, J. J. (2008). Limited iron isotope variations in recent lateritic soils from Nsimi, Cameroon: Implications for the global Fe geochemical cycle. *Chemical Geology*, *253*(1), 54–63. https://doi.org/10.1016/j.chemgeo.2008.04.011

Poulton, S. W., & Canfield, D. E. (2005). Development of a sequential extraction procedure for iron: Implications for iron partitioning in continentally derived particulates. *Chemical Geology*, *214*(3–4), 209–221. https://doi.org/10.1016/j.chemgeo.2004.09.003

Poulton, S. W., & Canfield, D. E. (2011). Ferruginous conditions: A dominant feature of the ocean through Earth's history. *Elements*, *7*(2), 107–112. https://doi.org/10.2113/gselements.7.2.107

Qi, M., Gao, T., Wang, Z., Liu, Y., Xia, Y., Song, C., et al. (2022). Iron solid-phase differentiation controls isotopic fractionation during lateritic weathering of basalt. *Catena*, *217*, 106512. https://doi.org/10.1016/j.catena.2022.106512

Raiswell, R., & Canfield, D. E. (2012). The iron biogeochemical cycle past and present. *Geochemical Perspectives*, *1*, 1–232. https://doi.org/10.7185/geochempersp.1.1

Retallack, G. J. (2010). Lateritization and bauxitization event. *Economic Geology*, *105*(3), 655–667. https://doi.org/10.2113/gsecongeo.105.3.655

Rouxel, O. J., Bekker, A., & Edwards, K. J. (2005). Iron isotope constraints on the Archean and Paleoproterozoic ocean redox state. *Science*, *307*(5712), 1088–1091. https://doi.org/10.1126/science.1105692

Saito, M. A., Noble, A. E., Tagliabue, A., Geopfert, T. J., Lamborg, C. H., & Jenkins, W. J. (2013). Slow-spreading submarine ridges in the South Atlantic as a significant oceanic iron source. *Nature Geoscience*, *6*(9), 775–779. https://doi.org/10.1038/NGEO1893

Sauzéat, L., Rudnick, R. L., Chauvel, C., Garçon, M., & Tang, M. (2015). New perspectives on the Li isotopic composition of the upper continental crust and its weathering signature. *Earth and Planetary Science Letters*, *428*, 181–192. https://doi.org/10.1016/j.epsl.2015.07.032

Scholz, F. (2018). Identifying oxygen minimum zone-type biogeochemical cycling in Earth history using inorganic geochemical proxies. *Earth-Science Reviews*, *184*, 29–45. https://doi.org/10.1016/j.earscirev.2018.08.002

Scholz, F., Beil, S., Flögel, S., Lehmann, M. F., Holbourn, A., Wallmann, K., & Kuhnt, W. (2019). Oxygen minimum zone-type biogeochemical cycling in the Cenomanian-Turonian Proto-North Atlantic across oceanic anoxic event 2. *Earth and Planetary Science Letters*, *517*, 50–60. https://doi.org/10.1016/j.epsl.2019.04.008

Scholz, F., McManus, J., Mix, A. C., Hensen, C., & Schneider, R. R. (2014). The impact of ocean deoxygenation on iron release from continental margin sediments. *Nature Geoscience*, *7*(6), 433–437. https://doi.org/10.1038/ngeo2162

Scholz, F., Schmidt, M., Hensen, C., Eroglu, S., Geilert, S., Gutjahr, M., & Liebetrau, V. (2019). Shelf-to-basin iron shuttle in the Guaymas basin, Gulf of California. *Geochimica et Cosmochimica Acta*, *261*, 76–92. https://doi.org/10.1016/j.gca.2019.07.006

Schuth, S., Hurraß, J., Münker, C., & Mansfeldt, T. (2015). Redox-dependent fractionation of iron isotopes in suspensions of a groundwater-influenced soil. *Chemical Geology*, *392*, 74–86. https://doi.org/10.1016/j.chemgeo.2014.11.007

Severmann, S., McManus, J., Berelson, W. M., & Hammond, D. E. (2010). The continental shelf benthic iron flux and its isotope composition. *Geochimica et Cosmochimica Acta*, *74*(14), 3981–4004. https://doi.org/10.1016/j.gca.2010.04.022

Sigman, D. M., & Boyle, E. A. (2000). Glacial/interglacial variations in atmospheric carbon dioxide. *Nature*, *407*(6806), 859–869. https://doi.org/10.1038/35038000

Sun, J., Zhu, X., Chen, Y., & Fang, N. (2013). Iron isotopic constraints on the Genesis of Bayan Obo ore deposit, Inner Mongolia, China. *Precambrian Research*, *235*, 88–106. https://doi.org/10.1016/j.precamres.2013.06.004

Tagliabue, A., Aumont, O., & Bopp, L. (2014). The impact of different external sources of iron on the global carbon cycle. *Geophysical Research Letters*, *41*(3), 920–926. https://doi.org/10.1002/2013gl059059

Teng, F.-Z., Dauphas, N., & Helz, R. T. (2008). Iron isotope fractionation during magmatic differentiation in Kilauea Iki lava lake. *Science*, *320*(5883), 1620–1622. https://doi.org/10.1126/science.1157166

Thompson, A., Ruiz, J., Chadwick, O. A., Titus, M., & Chorover, J. (2007). Rayleigh fractionation of iron isotopes during pedogenesis along a climate sequence of Hawaiian basalt. *Chemical Geology*, *238*(1), 72–83. https://doi.org/10.1016/j.chemgeo.2006.11.005

Tribovillard, N., Algeo, T. J., Lyons, T., & Riboulleau, A. (2006). Trace metals as paleoredox and paleoproductivity proxies: An update. *Chemical Geology*, *232*(1), 12–32. https://doi.org/10.1016/j.chemgeo.2006.02.012

Wang, D. H., Li, P. G., Qu, W. J., Yin, L. J., Zhao, Z., Lei, Z. Y., & Weng, S. F. (2013). Discovery and preliminary study of the high tungsten and lithium contents in the Dazhuyuan bauxite deposit, Guizhou, China. *Science China Earth Sciences*, *56*(1), 145–152. https://doi.org/10.1007/s11430-012-4504-2

Wang, Q., Liu, X., Yan, C., Cai, S., Li, Z., Wang, Y., et al. (2012). Mineralogical and geochemical studies of boron-rich bauxite ore deposits in the Songqi region, SW Henan, China. *Ore Geology Reviews*, *48*, 258–270. https://doi.org/10.1016/j.oregeorev.2012.04.004

Wang, Q., Yang, L., Xu, X., Santosh, M., Wang, Y., Wang, T., et al. (2020). Multi-stage tectonics and metallogeny associated with Phanerozoic evolution of the South China block: A holistic perspective from the Youjiang Basin. *Earth-Science Reviews*, *211*, 103405. https://doi.org/10.1016/j.earscirev.2020.103405

Wang, T., Zhao, X., Li, J., & Lv, T. (2014). Distribution characteristics of lithium in Yinkuangyakou bauxite deposit, Chongqing. *Contributions to Geology and Mineral Resources Research*, *29*, 541–545. https://doi.org/10.6053/j.issn.1001-1412.2014.04.010

Weng, S., Yu, W., Algeo, T. J., Du, Y., Li, P., Lei, Z., & Zhao, S. (2019). Giant bauxite deposits of South China: Multistage formation linked to late Paleozoic ice age (LPIA) eustatic fluctuations. *Ore Geology Reviews*, *104*, 1–13. https://doi.org/10.1016/j.oregeorev.2018.10.014

Wiederhold, J. G., Kraemer, S. M., Teutsch, N., Borer, P. M., Halliday, A. N., & Kretzschmar, R. (2006). Iron isotope fractionation during proton-promoted, ligand-controlled, and reductive dissolution of goethite. *Environmental Science & Technology*, *40*(12), 3787–3793. https://doi.org/10.1021/es052228y

Wiederhold, J. G., Teutsch, N., Kraemer, S. M., Halliday, A. N., & Kretzschmar, R. (2007a). Iron isotope fractionation during pedogenesis in redoximorphic soils. *Soil Science Society of America Journal*, *71*(6), 1840–1850. https://doi.org/10.2136/sssaj2006.0379

Wiederhold, J. G., Teutsch, N., Kraemer, S. M., Halliday, A. N., & Kretzschmar, R. (2007b). Iron isotope fractionation in oxic soils by mineral weathering and podzolization. *Geochimica et Cosmochimica Acta*, *71*(23), 5821–5833. https://doi.org/10.1016/j.gca.2007.07.023

Wu, B., Amelung, W., Xing, Y., Bol, R., & Berns, A. E. (2019). Iron cycling and isotope fractionation in terrestrial ecosystems. *Earth-Science Reviews*, *190*, 323–352. https://doi.org/10.1016/j.earscirev.2018.12.012

Wu, L., Percak-Dennett, E. M., Beard, B. L., Roden, E. E., & Johnson, C. M. (2012). Stable iron isotope fractionation between aqueous Fe(II) and model Archean ocean Fe–Si coprecipitates and implications for iron isotope variations in the ancient rock record. *Geochimica et Cosmochimica Acta*, *84*, 14–28. https://doi.org/10.1016/j.gca.2012.01.007

Yamaguchi, K. E., Johnson, C. M., Beard, B. L., Beukes, N. J., Gutzmer, J., & Ohmoto, H. (2007). Isotopic evidence for iron mobilization during Paleoproterozoic lateritization of the Hekpoort paleosol profile from Gaborone, Botswana. *Earth and Planetary Science Letters*, *256*(3–4), 577–587. https://doi.org/10.1016/j.epsl.2007.02.010

Yang, S., Wang, Q., Liu, X., Kan, Z., Santosh, M., & Deng, J. (2022). Global spatio-temporal variations and metallogenic diversity of karst bauxites and their tectonic, paleogeographic and paleoclimatic relationship with the Tethyan realm evolution. *Earth-Science Reviews*, *233*, 104184. https://doi.org/10.1016/j.earscirev.2022.104184

Yang, S. J., Wang, Q. F., Deng, J., Wang, Y. Z., Kang, W., Liu, X. F., & Li, Z. M. (2019). Genesis of karst bauxite-bearing sequences in Baofeng, Henan (China), and the distribution of critical metals. *Ore Geology Reviews*, *115*, 103161. https://doi.org/10.1016/j.oregeorev.2019.103161

Yang, S. J., Wang, Q. F., Lai, X. L., Qiao, L., Wang, R. X., Huang, Y. X., & Wang, Y. Z. (2021). Genesis of end-Guadalupian bauxite and pyrite deposits in the Youjiang Basin (South China): Insights into the causative link between magmatic events and mass extinction. *Journal of Asian Earth Sciences*, *215*, 104801. https://doi.org/10.1016/j.jseaes.2021.104801

Ye, L., Pan, Z. P., & Cheng, Z. T. (2008). The regularities of distribution of associated elements in Xiaoshanba bauxite deposit, Guizhou. *Acta Mineralogica Sinica*, *28*(2), 105–111. https://doi.org/10.16461/j.cnki.1000-4734.2008.02.010

Yesavage, T., Fantle, M. S., Vervoort, J., Mathur, R., Jin, L., Liermann, L. J., & Brantley, S. L. (2012). Fe cycling in the shale Hills critical zone observatory, Pennsylvania: An analysis of biogeochemical weathering and Fe isotope fractionation. *Geochimica et Cosmochimica Acta*, *99*, 18–38. https://doi.org/10.1016/j.gca.2012.09.029

Yu, W., Algeo, T. J., Du, Y., Zhang, Q., & Liang, Y. (2016). Mixed volcanogenic–lithogenic sources for Permian bauxite deposits in southwestern Youjiang Basin, South China, and their metallogenic significance. *Sedimentary Geology*, *341*, 276–288. https://doi.org/10.1016/j.sedgeo.2016.04.016

Yu, W., Algeo, T. J., Yan, J., Yang, J., Du, Y., Huang, X., & Weng, S. (2019). Climatic and hydrologic controls on upper Paleozoic bauxite deposits in South China. *Earth-Science Reviews*, *189*, 159–176. https://doi.org/10.1016/j.earscirev.2018.06.014

Yu, W., Wang, R., Zhang, Q., Du, Y., Chen, Y., & Liang, Y. (2014). Mineralogical and geochemical evolution of the Fusui bauxite deposit in Guangxi, South China: From the original Permian orebody to a Quaternary Salento-type deposit. *Journal of Geochemical Exploration*, *146*, 75–88. https://doi.org/10.1016/j.gexplo.2014.07.020

Yuste, A., Bauluz, B., & Mayayo, M. J. (2017). Origin and geochemical evolution from ferrallitized clays to karst bauxite: An example from the Lower Cretaceous of NE Spain. *Ore Geology Reviews*, *84*, 67–79. https://doi.org/10.1016/j.oregeorev.2016.12.025

Zamanian, H., Ahmadnejad, F., & Zarasvandi, A. (2016). Mineralogical and geochemical investigations of the Mombi bauxite deposit, Zagros Mountains, Iran. *Chemie der Erde-Geochemistry*, *76*(1), 13–37. https://doi.org/10.1016/j.chemer.2015.10.001

Zarasvandi, A., Carranza, E. J. M., & Ellahi, S. S. (2012). Geological, geochemical, and mineralogical characteristics of the Mandan and Deh-now bauxite deposits, Zagros fold belt, Iran. *Ore Geology Reviews*, *48*, 125–138. https://doi.org/10.1016/j.oregeorev.2012.02.01

Zhang, R., John, S. G., Zhang, J., Ren, J., Wu, Y., Zhu, Z., et al. (2015). Transport and reaction of iron and iron stable isotopes in glacial meltwaters on Svalbard near Kongsfjorden: From rivers to estuary to ocean. *Earth and Planetary Science Letters*, *424*, 201–211. https://doi.org/10.1016/j.epsl.2015.05.031

Zhang, S. Q., Liu, X. F., Zhao, F. H., Liu, D. N., Zou, Y., Zhang, W. X., et al. (2021). Geological and geochemical characteristics of karst bauxite-bearing sequences in Xiabu area, Central Shanxi Province, North China. *Journal of Geochemical Exploration*, *230*, 106849. https://doi.org/10.1016/j.gexplo.2021.106849

Zhang, Z., Zhou, L., Li, Y., Wu, C., & Zheng, C. (2013). The "coal-bauxite-iron" structure in the ore-bearing rock series as a prospecting indicator for southeastern Guizhou bauxite mines. *Ore Geology Reviews*, *53*, 145–158. https://doi.org/10.1016/j.oregeorev.2013.01.006

Zhao, L. H., Liu, X. F., Yang, S. J., Ma, X. L., Liu, L., & Sun, X. F. (2021). Regional multi-sources of Carboniferous karstic bauxite deposits in North China Craton: Insights from multi-proxy provenance systems. *Sedimentary Geology*, *421*, 105958. https://doi.org/10.1016/j.sedgeo.2021.105958

Zhu, X. K., Li, Z. H., Zhao, X. M., Tang, S. H., He, X. X., & Belshaw, N. S. (2008). High-precision measurements of Fe isotopes using MC-ICP-MS and Fe isotope compositions of geological reference materials. *Acta Petrologica et Mineralogica*, *27*, 263–272. https://doi.org/10.3969/j.issn.1000-6524.2008.04.001